



Contents lists available at ScienceDirect

Arabian Journal of Chemistry

journal homepage: www.ksu.edu.sa

A polyampholyte core-shell microgel as an environmentally sensitive drug carrier

Marcin Mackiewicz^{a,*}, Serife Dagdelen^a, Ewelina Waleka-Bargiel^{a,b}, Marcin Karbarz^{a,*}

^a Faculty of Chemistry, Biological and Chemical Research Center, University of Warsaw, 101 Żwirki i Wigury Av., PL 02-089 Warsaw, Poland

^b Faculty of Chemistry, Warsaw University of Technology, 3 Noakowskiego, PL 00-664 Warsaw, Poland

ARTICLE INFO

Keywords:

Drug delivery system
Core-shell
PEG
Cystamine
Controlled release
Redox degradation
pH and temperature sensitivity

ABSTRACT

In this study, we investigate a polyampholyte degradable core-shell (CS) microgel, with an anionic pH-sensitive core and a cationic pH- and temperature-sensitive shell, as a model system for drug delivery. The core was based on crosslinked poly(acrylic acid) and was synthesized through distillation precipitation polymerization. Then, the shell, based on cross-linked poly(poly(ethylene glycol) methyl ether methacrylate - N-(3-aminopropyl) methacrylamide), were built over the core via the seed polymerization. *N,N*-bis(acryloyl)cystamine was used as the linker for cross-linking both core and shell to give the core-shell particles the ability to degrade in the presence of reducing agent. The swelling characteristics of the core-shell microgels were studied using dynamic light scattering (DLS). The core-shell particles exhibited sensitivity to pH due to the presence of carboxylic and amine groups in the core and shell, respectively. The degradation of the core-shell particles was examined using electron microscopy and DLS. In the presence of glutathione, which acts as a reducing agent for the -S-S- bridges, commonly found in cancer cells, the particles underwent complete degradation. Our findings also demonstrate that the presence of the positively charged shell still enables efficient uptake of a drug in the form of a cation (doxorubicin DOX) into the anionic core and the drug can be released through the cationic shell. The release of DOX from the carrier was studied under different pH conditions to mimic the environment found in cancer cells. The results showed that at pH 7.4, the carrier exhibited the lowest release of DOX. However, under conditions mimicking the acidic and reducing environment typically for tumor microenvironment (pH 5.0 and $c_{\text{GSH}} = 40$ mM), the CS particles demonstrated the highest cumulative and sustained release of DOX. The results showed that the DOX-loaded particles exhibited increased cytotoxicity against MCF-7 cells, indicating enhanced anti-cancer activity. At the same time, these particles demonstrated reduced toxicity towards healthy MCF-10A cells, which suggests improved selectivity and reduced side effects. It is worth noting that the gel nanoparticles alone did not inhibit cell growth. Overall, these findings suggest that the DOX-loaded core-shell particles hold promise as a targeted drug delivery system, capable of preferentially releasing the drug in the acidic and reducing tumor microenvironment while minimizing toxicity towards healthy cells.

1. Introduction

Microgels are microparticles characterized by their colloidal stability, porous nature, and softness. They are composed of crosslinked polymer chains that swell within a suitable solvent (Agrawal and Agrawal, 2018; Karg, 2019). Polymer networks are typically obtained from synthetic polymers, natural polymers, or a combination of both (hybrid). For instance, microgels based on polysaccharides have gained prominence in delivering phototherapeutic agents for anticancer phototherapy, a treatment approach that has recently gained popularity

(Arjama, 2023; Xu, 2023). The synthesis of polysaccharide-based microgels involves processes such as cross-linking, self-assembly of amphiphilic polysaccharides, grafting and the formation of poly-electrolyte complexes (Arjama, 2023; Papagiannopoulos and Sotiropoulos, 2022; Praphakar, 2018; Chen, 2020; Praphakar, 2018). However its worth to mention that there are still important disadvantages of polysaccharide-based microgels. Some polysaccharide-based microgels may exhibit burst release behavior, where a significant portion of the encapsulated drug is released rapidly upon administration. This can lead to suboptimal drug delivery kinetics and potentially

* Corresponding authors.

E-mail addresses: mmackiewicz@chem.uw.edu.pl (M. Mackiewicz), karbarz@chem.uw.edu.pl (M. Karbarz).

<https://doi.org/10.1016/j.arabjc.2023.105464>

Received 20 July 2023; Accepted 16 November 2023

Available online 19 November 2023

1878-5352/© 2023 The Authors. Published by Elsevier B.V. on behalf of King Saud University. This is an open access article under the CC BY license (<http://creativecommons.org/licenses/by/4.0/>).

lower therapeutic efficacy. The size and structure of polysaccharide-based microgels can vary, which may affect their drug delivery performance. Variability can make it challenging to achieve consistent and predictable drug release profiles. From this perspective, microgels based on synthetic polymers appear more promising. These microgels can retain the inherent properties of their parent polymers while also acquiring advantageous new properties, depending on their specific architecture (Khan, 2018; Islam and Lyon, 2020; Shi, 2022; Akgonullu, 2023). The ability to tune microgel properties by introducing various chemical and structural features to them, as well as their well-defined size, easy synthesis and fast response (volume change) to external stimuli like temperature, pH and electromagnetic fields, make them prominent materials for various biomedical applications (Almeida, 2021; Tang, 2021; Li, 2021; Preman, 2021; Kubiak, 2022; Mackiewicz, 2021; Farooqi, 2017). In particular, their ability to uptake and release guest molecules makes them interesting carriers for delivery systems. Different guest molecules like proteins, enzymes, polyelectrolytes, drugs, surfactants can be loaded into microgels, and different interactions - electrostatic or hydrophilic/hydrophobic - between microgels and guest molecules can be observed (Mackiewicz, 2021; Waleka, 2020; Han, 2019; He, 2019; Xu, 2022; Wilson, 2022; Anooj, 2021). Moreover, there are many parameters that influence the colloidal stability of microgels and the uptake and release properties - such as the microgel architecture, the pH degree of ionization of the ionizable moieties of the microgel, spatial distributions of ionizable groups within the microgel, ionic strength and temperature of microgel dispersion (Malmsten, 2010; Pepe, 2017; Mackiewicz, 2019; Farmanbordar, 2021; Szafraniec-Szczesny, 2020; Yang and Zhao, 2019). Various microgel architectures can be synthesized, such as core-shell (CS) structures (Min, 2017; Gelissen, 2018).

Core-shell microgels, have emerged as a compelling area of focus in the field of pharmaceutical sciences. What sets them apart is their unique structural design, featuring a central core that accommodates therapeutic agents and an outer shell that serves as a protective barrier (Zhalechin, 2021). This design imparts several key advantages. Core-shell microgels exhibit an exceptional capacity for controlled and targeted drug release, driven by their sensitivity to environmental cues such as pH, temperature, and ionic strength. These properties are pivotal in medical applications, particularly in the treatment of cancer, where the goal is to maximize drug effectiveness while minimizing harm to healthy tissues (Lei, 2020; Mahdavi, 2020). Moreover, the ability to fine-tune core-shell microgels for specific drug loading and release kinetics makes them superior to other microgel systems. By harnessing these attributes, core-shell microgels hold the potential to revolutionize drug delivery strategies, enhancing treatment outcomes, and minimizing adverse side effects, thereby representing a significant advancement in the quest for more effective and patient-friendly therapeutic solutions.

For instance, a core-shell microgel may have a soft pH-responsive core surrounded by a neutral shell, or vice versa, have a soft neutral core and a charged shell. Richtering et al. synthesized polyampholyte *N*-isopropylacrylamide (NIPA) based microgels with a cationic core and an anionic shell as a carrier for anionic guest polyelectrolytes loaded with polystyrene sulfonate of different molecular weights (Gelissen, 2018). Islam and Lyon synthesized core-shell microgels by using seed-mediated, surfactant-free emulsion polymerization. This core-shell microgel consisted of a poly(*N*-isopropylacrylamide) (pNIPA) microgel core crosslinked with an *N,N'*-methylenebis(acrylamide) (BIS) and non-crosslinked poly(*N*-isopropylacrylamide-acrylic acid) (p(NIPA-AA)) shell. The authors postulated that a denser core region can be used to obtain a higher loading of encapsulated therapeutics, tracking dyes, or oligonucleotides (Islam and Lyon, 2020). Raju et al. reported the synthesis and properties of temperature- and pH-responsive p(NIPA-PEGMA)/p(NIPA-AA) CS nanogels with narrow size distributions, tunable sizes and increased drug loading efficiencies. These core-shell nanogels were synthesized using an optimized two-stage seeded polymerization methodology. Nanogels were loaded with 1-3,4-

dihydroxyphenylalanine (L-DOPA) and showed high loading and encapsulation efficiencies, opening up potential biomedical applications (Raju, 2018).

In this article, we report a study focusing on the synthesis, characterization and drug loading/releasing properties of a degradable, temperature- and pH-sensitive p(AA-BAC)/p(MEO₂MA-OEGMA-APMA-BAC) core-shell microgel with high drug loading capacity. The microgel showed high loading and encapsulation efficiencies of doxorubicin, an anticancer drug.

Distinguished from other polyampholyte drug delivery materials, the resulting core-shell microgel is characterized by exceptional biocompatibility and a unique feature: a VPTT (Volume Phase Transition Temperature) of 34 °C, which is close to human body temperature. What sets this core-shell microgel apart even further is its notably high carboxylic group content, a distinction rarely observed in existing literature mentioned above. This inherent feature confers pH sensitivity, an extensive capacity for loading anticancer drugs, and, consequently, the potential to serve as a markedly more efficient drug carrier system in the battle against cancer cells. Moreover, our core-shell microgels undergo degradation in the presence of glutathione. Glutathione is the reducing agent that present at elevated concentration in some cancer cells.

2. Experimental

2.1. Chemicals

Poly(ethylene glycol) methyl ether methacrylate (OEGMA, average M_n 500), di(ethylene glycol) methyl ether methacrylate (MEO₂MA), ammonium persulfate (APS), acrylic acid (AA, 99 %), *N,N'*-bis(acryloyl) cystamine (BAC), *N*-(3-aminopropyl) methacrylamide hydrochloride (APMA, 98 %), azobisisobutyronitrile (AIBN, 98 %), acetonitrile (ACN, 99.8 %), L-glutathione reduced (GSH) and doxorubicin hydrochloride (DOX) were supplied by Aldrich. NaOH, HCl and uranyl acetate were purchased from POCH. The ingredients were used in their original state without any purification. Water used for preparing all solutions was purified using a Hydrolab/HLP purification system. The final conductivity of the water was measured to be 0.055 $\mu\text{S cm}^{-1}$.

2.2. Materials for cell culture

Antibiotics, non-essential amino acids, trypsin/EDTA solution, fetal bovine serum and 3-(4,5-dimethylthiazol-2-yl)-2,5-diphenyltetrazolium bromide were supplied by Sigma Aldrich. Iscove's Modified Dulbecco's Media (IMDM), Minimum Essential Medium (MEM) (Biowest) and 2-propanol were purchased from Avantor Performance Materials Poland S.A. Phosphate buffered saline was supplied by General Chemistry Laboratory, IITD PAN.

2.3. Core-shell microgel synthesis

The p(AA-BAC) microgel was obtained by distillation polymerization using the procedure presented in our previous paper, and was used for preparation of the core-shell microgel (Mackiewicz, 2021). The p(AA-BAC)/p(MEO₂MA-OEGMA-APMA-BAC) core-shell microgel was then obtained using precipitation polymerization (Wolff, 2018; Karbarz, 2017) see Scheme 1. MEO₂MA (82.5 mol%), OEGMA (7.5 mol%), APMA (7 mol%), BAC (3 mol%), NaHCO₃ (5 mg), SDS (6 mg) and 4 mL of pAA microgel (27 mg/mL) - purified with dialysis, was combined with 25 mL of ionized water and transferred into a 250 mL three-neck flask. The flask was equipped with a reflux condenser, as well as inlet and outlet connections for inert gas. Additionally, a magnetic stirrer was placed inside the flask to facilitate agitation of the contents. Total MEO₂MA, OEGMA, APMA monomers and BAC linker concentration in the reactor was 37 mM. The mixture in the flask was purged with inert gas - argon, for a duration of 30 min. Then temperature was increased to 80 °C and an initiator - APS (9 mg dissolve in 2 mL H₂O 1.3 mM) with TEMED (30

μL 6.4 mM) - was added to initiate polymerization. The reaction was conducted under an inert gas blanket for a duration of 5 h. Throughout the polymerization process, the stirring rate was maintained at 250 rpm. The final pH equaled 7.

The microgel was purified through dialysis using a dialysis bag with a molecular weight cutoff of 10 kDa (Spectra/Por®). The samples were dialyzed with 5 L of water at room temperature for one week, with daily water changes. Then the core-shell particles were cleaned by centrifugation to separate them from possible nanogel particles obtained from shell material. Concentration of core-shell was estimated gravimetrically by measuring the mass of dry core-shell particles and it was equaled 5 mg/mL. Synthesis of core-shell particles was performed at different pHs: 3.0, 7.0 and 11.0. However, only at pH 7.0 aggregation of particles was not observed. The structures of the monomers and the method of synthesis of the core-shells are presented in Scheme 1.

2.4. Instrumental

2.4.1. Dynamic light scattering

The hydrodynamic diameter of the particles was determined using a Malvern Zetasizer instrument (Nano ZS, UK). The instrument was equipped with a 4 mW Helium-Neon laser, which emitted light at a wavelength of 632.8 nm, and a scattering angle of 173° was used for the measurements. Before taking the measurements, the samples (1 mL of dispersion of suitable pH in acrylic cuvette) were allowed to equilibrate at the desired temperatures for 5 min. The changes in particle hydrodynamic diameter were then measured as a function of temperature. The zeta potential was measured using the same instrument. A folded capillary cell with gold electrodes was employed for this purpose. The analyzer calculated the zeta-potential from the electrophoretic mobility using the Henry equation and the Smoluchowski approximation.

2.4.2. Fourier transform infrared (FTIR)

The FTIR spectra were recorded using a Fourier Transform Infrared Spectrometer (Perkin Elmer BX) located in Waltham, MA, USA. The instrument was equipped with a universal attenuated total reflectance (ATR) accessory, which allows for convenient and efficient sample analysis.

2.4.3. Electron microscopy (SEM and TEM)

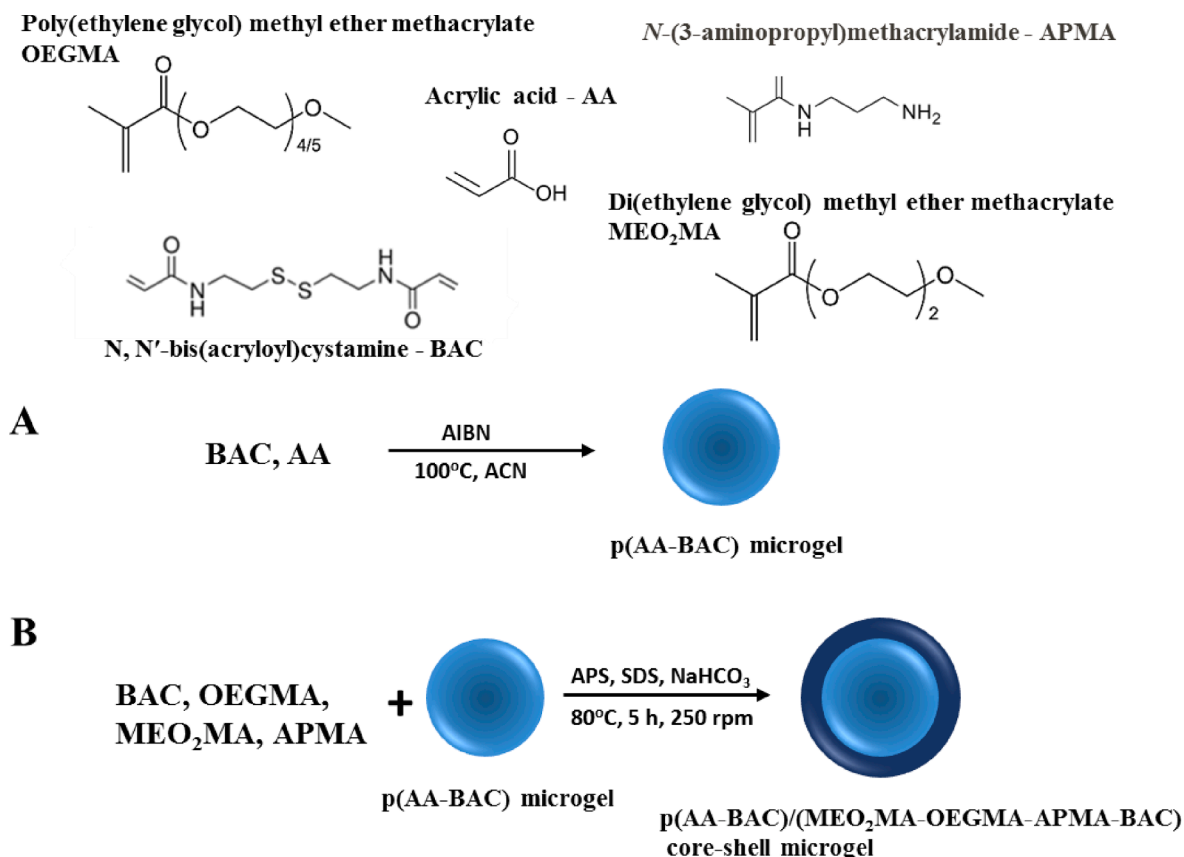
SEM micrographs were obtained using a Merlin instrument manufactured by Zeiss. The instrument was operated at 3 kV. To prepare the samples, a drop of gel dispersion was placed on the SEM table and allowed to dry at room temperature. Prior to imaging, the samples were coated with a 3 nm layer of Au-Pd alloy using a Mini Sputter Coater (Polaron SC7620) under vacuum conditions. TEM micrographs were captured using a Zeiss Libra 1200 instrument. A drop of gel dispersion was placed on a formvar-coated copper grid, and the samples were left to dry at room temperature. Subsequently, the grid with the dried samples was used for TEM imaging.

2.5. Other measurements

The pH of the aqueous dispersion of CS microgels was controlled by adding either sodium hydroxide or hydrochloride solution, and the pH was monitored using a Mettler Toledo model SevenGo-SG2 pH meter just before the measurements. The ionic strength of the suspensions was maintained at a constant value of 0.01 M. In experiments involving the use of GSH as a reducing agent, the pH of the suspensions was adjusted to approximately 5.0.

2.6. Loading and release of drug

Doxorubicin (DOX), an anticancer drug, was chosen to investigate



Scheme 1. Synthesis of p(AA-BAC)/p(MEO₂MA-OEGMA-APMA-BAC) core-shell microgel.

the usefulness of the p(AA-BAC)/p(MEO₂MA-OEGMA-APMA-BAC) core-shell microgel in drug delivery. The gel was dispersed in 4 mL of phosphate buffer solution (pH 7.4; 0.1 M), with a gel quantity of 1 mg. After dispersing the gel, 3.0 mg of DOX was added to the solution. The obtained solution was heated at 37 °C for 10 min and then cooled at 25 °C for 10 min; the process was repeated three times for consistency. After being kept at room temperature overnight, the solution was subjected to dialysis to separate and collect the CS microgel loaded with DOX, while simultaneously removing any free DOX present.

To evaluate the drug release from the gel, dialysis was employed. In this procedure, 0.25 mg of DOX + gels were put in 1 mL of either acetate buffer (pH 5.0, 0.1 M) or phosphate buffer (pH 7.4, 0.1 M), and then placed within dialysis tubes with a molecular weight cutoff (MWCO) of 10 kDa. These tubes were subsequently immersed in 9 mL of suitable buffer (37 °C, 100 rpm), without or with GSH (40 mM) and the absorbance of the buffers at 480 nm was measured to calculate mass of released doxorubicin. To examine the loading and release of DOX from gels the absorbance of the solution at 480 nm was measured and the concentrations of DOX were determined from the calibration curve.

2.7. Cell examination

2.7.1. Cell culture

The MCF-7 breast adenocarcinoma cells and HT-29 colorectal adenocarcinoma cells were purchased from the European Collection of Authenticated Cell Cultures (ECACC). The MCF-7 cells were maintained in IMDM medium, while the HT-29 cells in MEM medium supplemented with fetal bovine serum (10 % (MCF-7) or 5 % (HT-29)), antibiotics: 100 U/mL penicillin, 100 µg/mL streptomycin, 250 µg/mL amphotericin B, and non-essential amino acids (0.1 mM) at 37 °C in humidified incubator with a 5 % carbon dioxide atmosphere.

2.7.2. Cell viability assay

Cell viability was determined using MTT (3-(4,5-dimethylthiazol-2-yl)-2,5-diphenyltetrazolium bromide) colorimetric assay. After reaching the confluence of 80 %, the cells were trypsinized with 0.25 % trypsin/EDTA solution and seeded in 96-well plates (Cytogen) at a density of 40,000 and 60,000 cells/mL for the MCF-7- and HT-29 cells, respectively. After 24 h, the medium containing DOX, the gel and the gel containing DOX (at increasing concentration) was added to the cells, which were further incubated for 72 h. After that incubation time, the cells were washed with PBS and 50 µL/well of MTT solution (5 mg/1mL PBS) were added to each well. In order to dissolve the formazan crystals, 200 µL of 2-propanol were added after 3 h of incubation. The absorbance was measured at 570 nm with a ELX800 Absorbance Microplate Reader (BioTek Instruments).

2.7.3. IC50 calculation

The IC₅₀ values for DOX and gel containing DOX (the concentration that inhibited cell viability to 50 % of the control cells) were determined using GraphPad Prism 7 (GraphPad Software) and the nonlinear regression analysis of the best fit Hill slope curve. The values are expressed as the mean value ± standard deviation (S.D.) from two independent experiments (n = 6).

3. Results and discussion

The FTIR technique was employed to characterized the polymerization products. In the IR spectra, bands corresponding to all characteristic functional groups were observed (see Fig. 1). The bands at 1452 cm⁻¹, 1726 cm⁻¹, and 3338 cm⁻¹ are ascribed to COO⁻, C=O, and OH of the pAA hydrogel. The band at 3338 cm⁻¹ is also assigned to N-H stretching. The bands observed in a range of 3000–2800 cm⁻¹ could be attributed to the asymmetric and symmetric vibrations of -CH₃, -CH₂- and -CH(R)₂ groups. Characteristic signals of OEGMA, MEO₂MA mers are located at 1110 cm⁻¹ (C-O stretching) and 861 cm⁻¹ (C-O-C

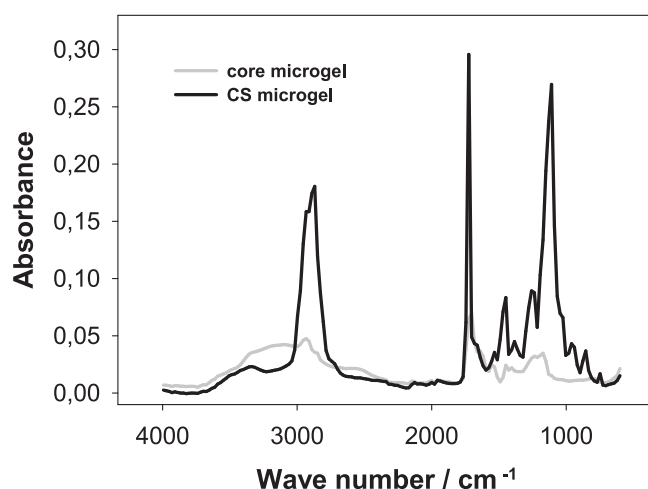


Fig. 1. Representative FTIR absorbance spectrum for p(AA-BAC) core microgels and p(AA-BAC)/p(MEO₂MA-OEGMA-APMA-BAC) core-shell microgels.

stretching) (Xu, 2022). Absorption peak at 1452 cm⁻¹ is related to the stretching vibrations of C-N groups of BAC and APMA while band at 749 cm⁻¹ is attributed waging vibrations of N-H groups in APMA and is observed only for primary and secondary amines.

The morphology of the core and core-shell particles was examined by electron microscopy. Scanning electron microscopy (SEM) (see Fig. 2 C and D) and transmission electron microscopy (TEM) were used for this purpose (see Fig. 2 A and B). As is evident in the SEM micrographs, both the dried core and CS particles formed spherical and monodisperse particles. The formation of shells is evidenced by the larger sizes of the CS gels compared to the not-modified gels. The mean diameter of the dried particles measured from the SEM and TEM were similar, at approx. 250 nm and 370 nm for core and core-shell, respectively. Independently, the staining technique with uranyl acetate (UO₂Ac₂) was employed to visualize the distribution of the anionic groups; COO⁻ groups appeared darker in the TEM images. In the presented TEM micrographs, the cores and the cores of the core-shell microgel particles are completely black, which means gel particles exhibit a uniform distribution of carboxylic groups within their polymer network. Moreover in the case of the CS particles, a thin shell is observed.

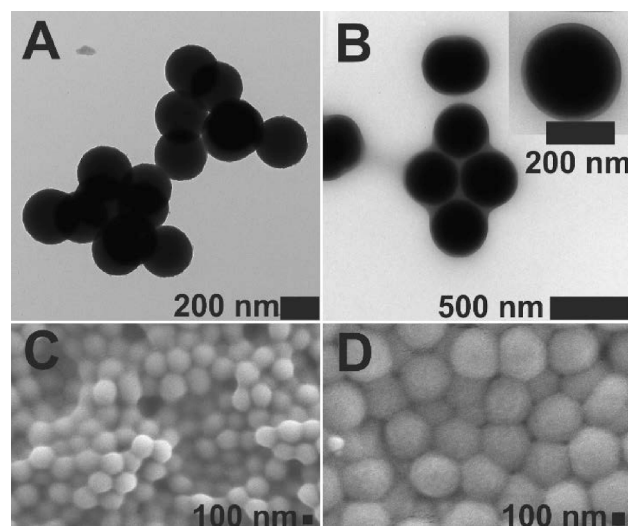


Fig. 2. TEM (A) and SEM (C) micrographs of p(AA-BAC) core microgels, and TEM (B) and SEM (D) images of p(AA-BAC)/p(MEO₂MA-OEGMA-APMA-BAC) core-shell microgels. Uranyl acetate 2 % solution was utilized to stain the particles intended for transmission electron microscopy (TEM).

Next, the effect of pH on the size, volume phase transition temperature (VPTT), and stability of the core-shell microgel was assessed. The diameter of the core-shell microgel particles at various temperatures and pH values was determined using the dynamic light scattering technique. The results are presented in Fig. 3. It can be seen that the hydrodynamic diameter of core-shell microgels decreased with an increase in temperature. At temperatures below the VPTT, the temperature-sensitive shell of the material was in a swollen state. However, as the temperature rose above the VPTT, the shell transitioned to a shrunken state. The described behavior is commonly observed in thermo-sensitive gels that are constructed using polymers exhibiting a lower critical solution temperature (LCST). These gels tend to undergo a transition from a swollen state to a shrunken state as the temperature surpasses the LCST (Lutz, 2008). However, as can be seen in Fig. 3, not only the temperature but the pH value also has major influence on the swelling behavior of the core-shells, due to the pH sensitive p(AA-BAC) core and, pH and temperature sensitive p(MEO₂MA-OEGMA-APMA-BAC) shell. At pH higher than the pKa of pAA (pKa ~ 4.5), the core should be in the swollen state, due to the prevalence of ionized carboxyl groups (Wisniewska, 2014). At pH lower than the pKa of pAA, on the other hand, the core should be in the shrunken state due to the prevalence of protonated carboxylic groups in the polymeric network. The opposite behavior should be seen for the shell. At pH lower than the pKa of APMA (pKa = 8.3), the shell should be in the swollen state due to the ionized amine groups in the polymer

network, while at pH values higher than the pKa of APMA, the shell should be in the shrunken state (Lago, 2011). Importantly, the core consists mainly of carboxylic groups, whereas the amount of amine groups from APMA (7 mol%) in the shell is small, and so differences in size, in response to pH, should be more visible for the core, after shrinking of the shell. At pH 2.8 and pH 5.2, which is lower and near the pKa of pAA, respectively, more carboxylic groups in the core of the core-shell particles are protonated than at higher pHs (7.7 and 10.7), thus at temperatures higher than the volume phase transition of core-shell, the size of particles was smaller at lower pH; at pH 2.8 the size of core-shell particles after volume phase transition corresponds well with the size of unmodified core at these pH values (see Fig. 3 inset). Moreover, with decrease of pH, increase of volume phase transition of core-shell was observed. As pH decrease, more amine groups in the temperature and pH sensitive shell are protonated and a higher temperature is needed for shrinking of the particles. The zeta potentials of both the core and the core-shell particles were determined. It was observed that at pH 5.8, the zeta potential was -34 mV for the core and 12 mV for the core-shell particles, respectively. These findings confirm that the negatively charged core is surrounded by a positively charged shell.

Colloidal stability of CS particles was also examined. For this purpose, the size distribution of particles was measured at different salt concentrations and different times of microgel interaction with salt at physiological concentration (0.15 M) (Fig. 3B). All experiments were conducted at body temperature. As seen in Fig. 3B, particles remained stable at all measured concentrations of salt, with only a slight, non-significant decrease in particle size observed from 777 nm to 644 nm at 0.01 M and 0.7 M of NaCl, respectively. The measurement of time-dependent colloidal stability of the microgel demonstrated very good stability; the microgel did not change in size even after 2 weeks of interaction with salt (0.15 M - physiological salt concentration) - Fig. 3B inset.

The degradation of the core-shell particles was also investigated by the DLS technique. The particles were treated with a reducing agent, glutathione (GSH - 40 mM), which exist in most tumor cells at high level (Gamcsik, 2012). Glutathione has a reducing effect because of its thiol group (-SH). When glutathione encounters disulfide bonds (-S-S-) within the core-shell particles, it can donate electrons through its thiol group (Zhang, 2021; Chakravarthi, 2006). This donation leads to the reduction of these bonds and the subsequent degradation of the particles, releasing their cargo, in our case doxorubicin. The changes in core-shell size, in the presence of GSH (40 mM), are presented in Fig. 4. Fig. 4 illustrates a reduction in the size of the core-shell structure upon the introduction of GSH. This decrease can be attributed to the disruption or

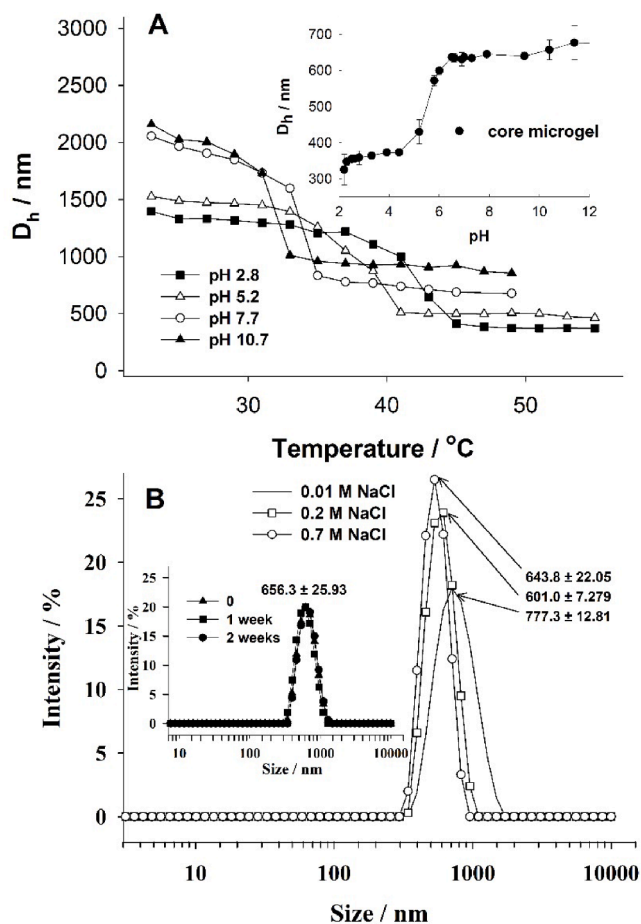


Fig. 3. A - a plot of the hydrodynamic diameter (D_h) as a function of temperature for p(AA-BAC)/p(MEO₂MA-OEGMA-APMA-BAC) core-shell microgel in different pHs. Inset A - hydrodynamic diameter for the core microgel measured at 20 °C, as a function of pH. B - Size distribution of core-shell particles measured at different salt concentration at 37 °C. Inset B - size distribution of core-shell particles measured after different time interaction of CS microgel with 0.15 M NaCl at 37 °C.

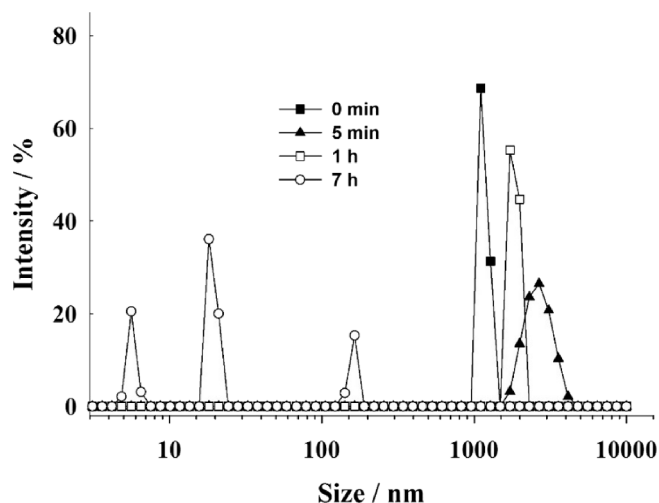


Fig. 4. Evolution of core-shell particle diameter distribution after being exposed to 40 mM GSH at 25 °C. Data from DLS measurements.

destruction of the particle structure caused by the reduction process. However, at the beginning of the reaction an increase in the size of particles was observed - probably caused by relaxation and swelling of the net of particles due to breaking of some -S-S- bridges. After 1 h of reaction, the diameter of particles started to decrease, and after 7 h nearly complete degradation of the core-shell into particles of different size was observed; cleavage of the remaining -S-S- bonds.

Compared to indirect methods of assessing particle degradation, such as analyzing transmittance or size, TEM and SEM offer the advantage of directly visualizing any alterations in particles morphology following degradation. To investigate the disassembly of the CS structure resulting from the reduction of -S-S- bridges, we utilized 40 mM GSH. Fig. 5 displays representative images. Visible in Fig. 5, prior to the interaction with GSH, the CS particles exhibited a spherical shape and remained intact (Fig. 5A and 5C). However, after one day of incubation in the presence of GSH, notable morphological alterations were observed (Fig. 5B and 5D). As observed in SEM images, the particle surfaces were extensively damaged. TEM images further confirm the absence of spherical structures, revealing only the presence of very finely fragmented irregular polymeric structures. The reduction of -S-S-bridges by the reducing agent led to the disintegration of the CS particles, resulting in the formation of fragmented structures. The original spherical shape and surface of the particles were fully disrupted.

Next, the usefulness of the core-shell microgel as a doxorubicin (anti-cancer drug) carrier was examined. Loading of doxorubicin was conducted at pH 7.4. At this pH, doxorubicin is electrostatically bound to the polymeric network of core-shells; the ionized carboxylic groups in core of the core-shell attract the protonated amine groups of doxorubicin. Drug loading capacity (DLC) was evaluated using the equation:

$DLC\% = \frac{m_{total}^{DOX} - m_{free}^{DOX}}{m_{CS/DOX}} \times 100\%$, where m_{total}^{DOX} is the overall mass of drug utilized during the loading procedure, m_{free}^{DOX} is the unbound mass of drug, and $m_{CS/DOX}$ is the mass of the core-shell after loading with the drug. The calculated Drug Loading Capacity (DLC) was approximately 300 %. The loading efficiency (LE) was assessed using the following equation:

$$LE\% = \frac{m_{total}^{DOX} - m_{free}^{DOX}}{m_{total}^{DOX}} \times 100\%, \text{ and it was approx. } 99\%.$$

Next, we investigated the impact of pH and GSH on the release efficiency of DOX from the core-shell. The experiments were conducted at a temperature of 37 °C, and the outcomes are depicted in Fig. 6. It is evident in Fig. 6 that the release profiles were observed to be dependent

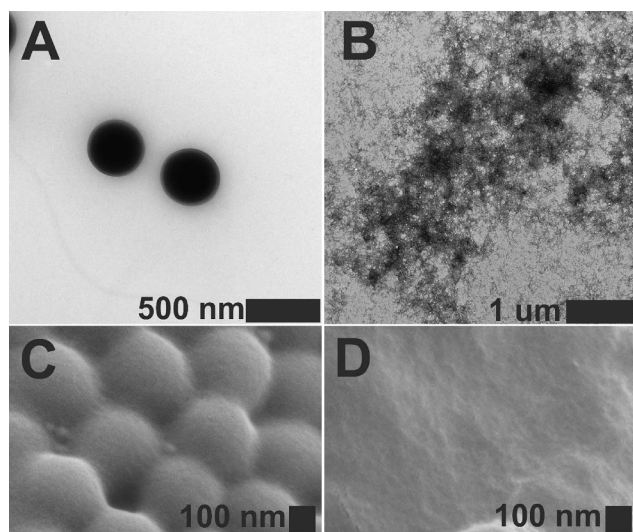


Fig. 5. TEM (A) and SEM (C) images of core-shell microgel particles before degradation and TEM (B) and SEM (D) images of core-shell degradation products obtained after one day of interaction with 40 mM GSH (pH 5.0). Particles for TEM were treated with a 2 % uranyl acetate solution to enhance contrast.

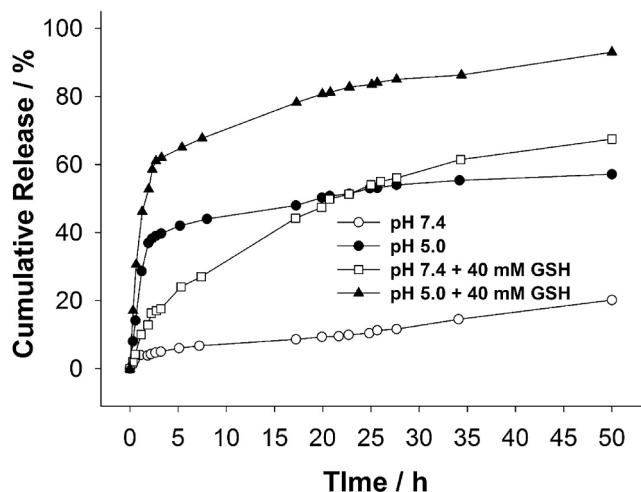


Fig. 6. Release profiles of DOX from p(AA-BAC)/p(MEO₂MA-OEGMA-APMA-BAC) core-shell microgel were examined in buffered solutions at 37 °C. Glutathione was introduced at the concentrations specified in the graphs.

on the pH of the solution and the presence of the reducing agent. The smallest amount of drug was released from the core-shells at pH 7.4 in the absence of GSH. At a pH of 7.4, the majority of carboxylic groups within the polymer network carried a negative charge, while drug was positively charged due to protonation of its amino groups. The electrostatic attractions between drug and the core of the core-shell caused only approximately 20 % of drug to be released at pH 7.4. However, at a lower pH of 5.0, a significantly higher cumulative release was observed, characterized by a burst or fast release. Without the presence of GSH and after a few hours, the cumulative release at pH 5.0 increased to approximately 40 %. After two days, it further increased to around 55 %. At pH 5.0, the electrostatic interactions between drug and the core-shell became weaker because some of the carboxylic groups in the core-shell were protonated. Consequently, almost three times more drug was released at pH 5.0 compared to pH 7.4. However, upon the addition of a reducing agent, both burst/fast release and sustained release were observed in both buffers containing GSH. Initially, within the first few hours, a fast release occurred as the polymer network of the core-shell was loosened and damaged by GSH. Subsequently, a slow and long-term release of DOX was observed, attributed to further degradation of the core-shell. After a 3 h incubation period in pH 7.4 with GSH and pH 5.0 with GSH, the cumulative release increased to approximately 17 % and 63 %, respectively. After 24 h, the cumulative release further increased to around 58 % in pH 7.4 with GSH and 85 % in pH 5.0 with GSH, and the release efficiency continued to improve. It is important to note that in the absence of GSH, sustained release was practically negligible. The combination of pH 5.0 and GSH significantly enhanced the efficiency of the drug releasing, owing to the synergistic effect of loosening the core-shell structure and weakening the interactions between drug and carboxylic groups.

It is crucial to note that incorporating cationic units into the microgel structure offers exciting possibilities for drug delivery. With both anionic and cationic components within the same carrier, the loading of various anti-cancer drugs becomes possible, each exhibiting its own charge characteristics. This dual-drug loading capability enables the delivery of multiple therapeutic agents, each with distinct mechanisms of action. In the battle against complex diseases like cancer, combining drugs can enhance treatment efficacy by targeting cancer cells through multiple pathways, potentially reducing the likelihood of resistance. Next step can involve loading a negatively charged anticancer drug onto the cationic unit of the core-shell microgel. Additionally, amine groups can be modified with folic acid, a cancer-targeting agent.

To evaluate the potential cytotoxicity of the selected materials

towards cancer cells (MCF-7) and healthy cells (MCF-10A), both cell types were incubated with various concentrations of the tested compounds for 72 h, followed by the MTT assay. Fig. 7A and 7B illustrate the results, indicating that the core-shell particles displayed no toxicity towards the cells across the whole range of concentrations subjected to testing. The viability of both MCF-10A and MCF-7 cells remained at 80 % or higher for all concentrations of the core-shell particles, indicating excellent biocompatibility of the not-loaded CS. In comparison to not-loaded CS, an inverse relationship between cell viability and drug concentration was observed for core-shell particles loaded with drug and free drug. As the drug concentration increased, the cell viability decreased. For the MCF-7 cell lines the IC₅₀ value was equal to 0.21 μM and 0.20 μM for free drug and drug loaded core-shell microgels, respectively (see Fig. 7 A). That mean the CS loaded with DOX was a little more toxic than DOX alone. Interesting findings were observed for MCF-10A cells. (see Fig. 7 B). Remarkable preservation of the healthy cells was accomplished. When DOX alone was administered, the IC₅₀ value was observed to be 0.16 μM . However, when the healthy cells were incubated with the drug-loaded carriers, a substantial decrease in cytotoxicity was observed, with the IC₅₀ value reaching 8.65 μM . This means that higher selectivity of CS microgels loaded with DOX for

cancer cells compared to healthy cells is observed.

To evaluate the effect of carriers on the selected cells, also confocal microscopy was employed. Fig. 8 displays the images of MCF-7 and MCF-10A cells after 72 h of treatment with the CS loaded with the drug. The images reveal that in healthy cells (MCF-10A), the DOX primarily appeared in the cytoplasm. Conversely, in cancer cells (MCF-7), DOX was accumulated in the nuclei.

The differences between the impact of the free drug and DOX loaded CS microgel against MCF-10A healthy cells was determined. The concentration of DOX in both cases equaled 0.01 μM . The difference between morphologies of the healthy cells treated with DOX alone and DOX loaded CS microgel appeared, see Fig. 9. In the case of free DOX the cells were smaller and round, whereas in the CS microgel loaded with the cells kept their natural, elongated shape. Taking into account the results of the above examination it can be concluded that the effectiveness of the microgels as the carriers targeting the cancer cells can be considered as satisfactory.

4. Conclusions

We successfully obtained a novel type of degradable core-shell

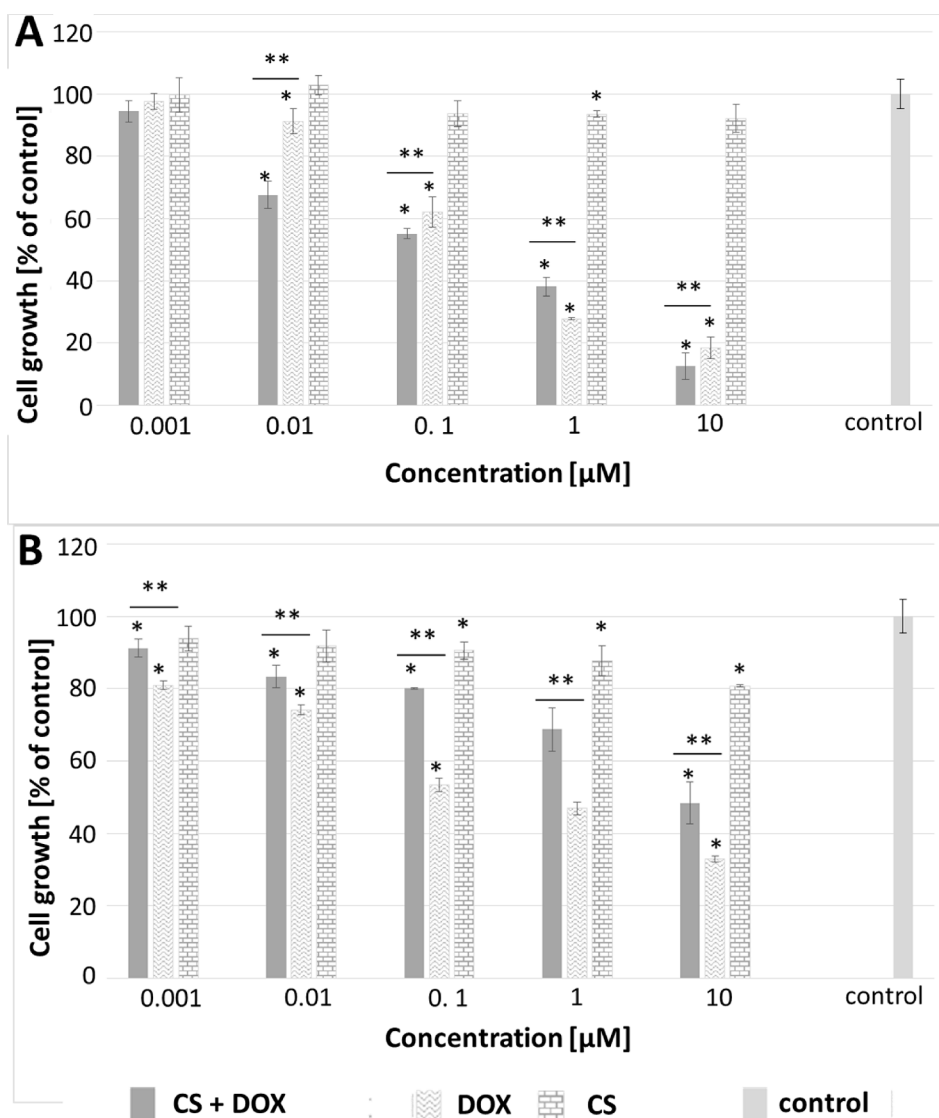


Fig. 7. MTT assay results analyzed using one-way ANOVA for MCF-7 (A) and MCF-10A (B) cell lines after 72-hour treatment with free doxorubicin, free CS particles and CS loaded with doxorubicin (CS + DOX). “*” indicates differences from the control sample, “**” denotes differences between groups. A difference was considered significant for P values < 0.05.

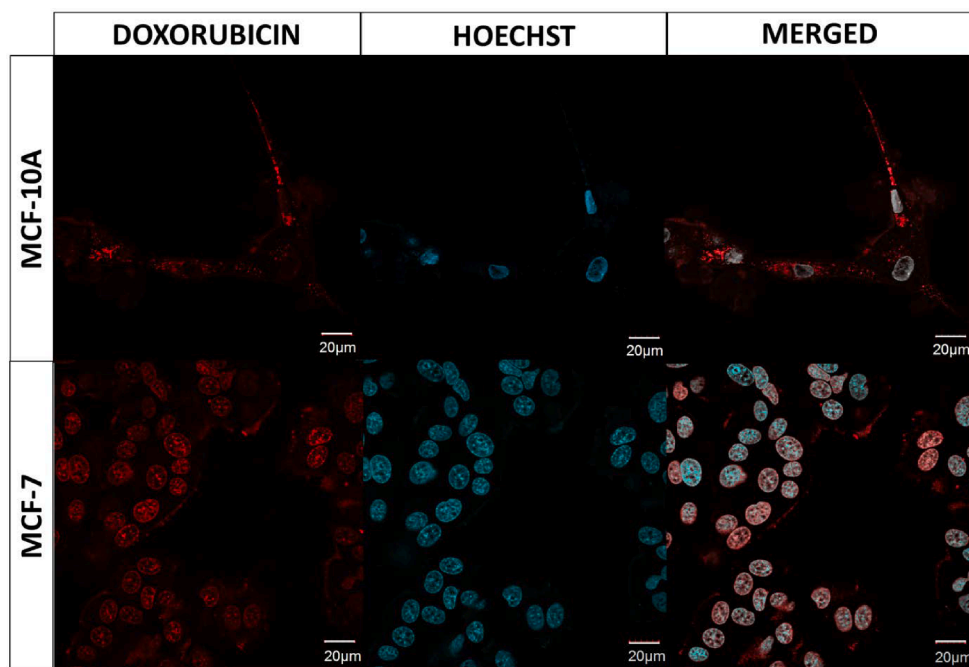


Fig. 8. Confocal images of MCF-10A and MCF-7 cell lines after 72 h of treatment with DOX + CS. The nuclei of cells were stained with fluorescent dye - Hoechst, resulting in a blue color. For each cell line, the figure presents separate fluorescent signals as well as a merged signal. The red color represents the fluorescence emitted by doxorubicin. Please refer to the web version of this article for a detailed interpretation of the references to color in the figure legend. (For interpretation of the references to color in this figure legend, the reader is referred to the web version of this article.)

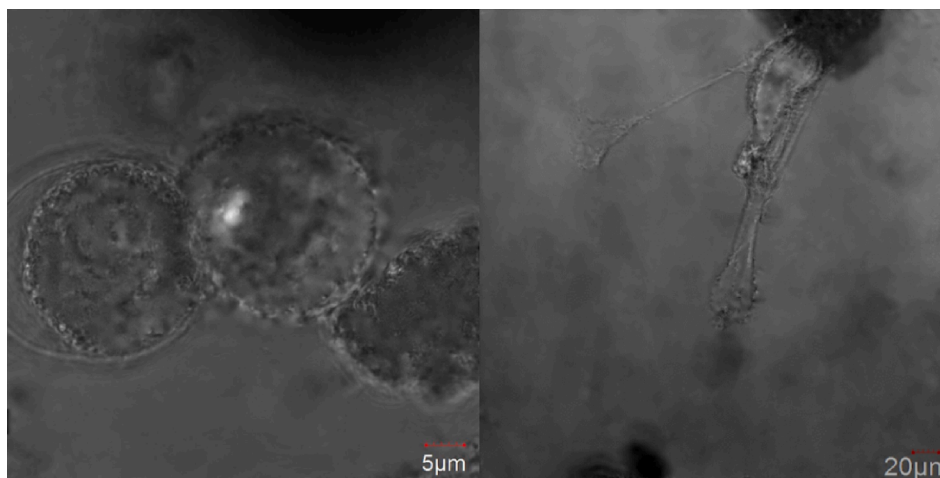


Fig. 9. Confocal images of MCF-10A cells treatment with doxorubicin (left) and doxorubicin loaded into core-shell microgels (right).

microgels, with an anionic pH-sensitive core and a cationic pH- and temperature-sensitive shell, and demonstrated their potential to be used as an efficient cancer drug carrier. First, cores based on poly(acrylic acid) crosslinked with *N,N'*- bis(acryloyl)cystamine were synthesized using distillation precipitation polymerization. Next, the cores were covered by poly(poly(ethylene glycol) methyl ether methacrylate - *N*-(3-aminopropyl)methacrylamide) also crosslinked with BAC via seed precipitation polymerization. Poly(ethylene glycol) chains gave the core-shells thermosensitivity, the carboxylic and amine groups were responsible for the pH sensitivity of the particles, while the linker provided the core-shell redox sensitivity. The abundance of carboxylic groups in the core of the core-shells allowed it to bind DOX due to electrostatic interactions. The was very high, at approx. 300 %. During incubation in 40 mM of GSH the core-shell microgels slowly degraded and exhibited long-term release of the DOX. The maximum release of

DOX occurred at pH 5.0 when accompanied by GSH (glutathione). The drug-loaded core-shell microgels exhibited higher cytotoxicity compared to the free drug when tested on the cancer cells under examination. Significantly, the DOX drug within the carrier showed reduced toxicity towards healthy cells in comparison to the free drug. Additionally, the gel nanoparticles without drug were found to be non-toxic to the cells, further indicating the biocompatibility of the carrier material. The results of *in vitro* experiments indicated that the CS microgel is a good candidate to be applied as an effective carrier of drug. The demonstrated new mode of pH sensitivity of core-shells and the improved drug release in environmental of cancer cells may be useful in construction of “smart” carriers for targeted drug delivery.

Declaration of competing interest

The authors declare that they have no known competing financial interests or personal relationships that could have appeared to influence the work reported in this paper.

Acknowledgment

This work was supported by the National Science Center of Poland under grant number 2018/31/B/ST5/02859.

References

- Agrawal, G., Agrawal, R., 2018. *Small* 14, 39.
- Akgonullu, D.Z., et al., 2023. *Adv. Colloid Interfac.* 320.
- Almeida, F.S., et al., 2021. *Food Biophys.*
- Anooj, E.S., et al., 2021. *J. Mol. Struct.* 1239.
- Arjama, M., et al., 2023. *J. Pharm. Sci.-Us* 112 (6), 1603.
- Chakravarthi, S., et al., 2006. *EMBO Rep.* 7 (3), 271.
- Chen, G., et al., 2020. *Int. J. Pharmaceut.* 589.
- Farmanbodar, H., et al., 2021. *New J. Chem.* 45 (46), 21824.
- Farooqi, Z.H., et al., 2017. *Arab. J. Chem.* 10 (3), 329.
- Gamsik, M.P., et al., 2012. *Biomarkers* 17 (8), 671.
- Gelissen, A.P.H., et al., 2018. *Soft Matter* 14 (21), 4287.
- Han, X.X., et al., 2019. *Nanotechnology* 30, 5.
- He, L., et al., 2019. *J. Colloid Interf. Sci.* 541, 30.
- Islam, M.R., Lyon, L.A., 2020. *Colloid Polym. Sci.* 298 (4–5), 395.
- Karbarz, M., et al., 2017. *Appl. Mater. Today* 9, 516.
- Karg, M., et al., 2019. *Langmuir* 35 (19), 6231.
- Khan, J., et al., 2018. *Arab. J. Chem.* 11 (6), 897.
- Kubiak, A., et al., 2022. *Appl. Sci.-Basel* 12, 1.
- Lago, M.A., et al., 2011. *J. Funct. Biomater.* 2 (4), 373.
- Lei, B., et al., 2020. *Colloid Surface B* 193.
- Li, Z.G., et al., 2021. *J. Control. Release* 335, 541.
- Lutz, J.F., 2008. *J. Polym. Sci. Pol. Chem.* 46 (11), 3459.
- Mackiewicz, M., et al., 2019. *Eur. Polym. J.* 118, 606.
- Mackiewicz, M., et al., 2021. *Polym. Degrad. Stabil.* 190.
- Mahdavi, Z., et al., 2020. *RSC Adv.* 10 (31), 18280.
- Malmsten, M., et al., 2010. *Curr. Opin. Colloid In* 15 (6), 435.
- Min, W.F., et al., 2017. *Colloid Surface B* 152, 260.
- Papagiannopoulos, A., Sotiropoulos, K., 2022. *Polymers-Basel* 14, 4.
- Pepe, A., et al., 2017. *Sci Rep-Uk* 7.
- Praphakar, R.A., et al., 2018. *Int. J. Biol. Macromol.* 118, 1627.
- Praphakar, R.A., et al., 2018. *J. Mater. Chem. B* 6 (10), 1519.
- Preman, N.K., et al., 2021. *ACS Omega* 6 (8), 5075.
- Raju, R., et al., 2018. *Polymers-Basel* 10, 3.
- Shi, D.L., et al., 2022. *Arab. J. Chem.* 15, 1.
- Szafraniec-Szczesny, J., et al., 2020. *Polymers-Basel* 12, 9.
- Tang, L., et al., 2021. *Prog. Mater. Sci.* 115.
- Waleka, E., et al., 2020. *Int. J. Pharmaceut.* 579.
- Wilson, R.J., et al., 2022. *Particuology* 64, 85.
- Wisniewska, M., et al., 2014. *Colloid Polym. Sci.* 292 (3), 699.
- Wolff, H.J.M., et al., 2018. *Acs Appl. Mater. Inter.* 10 (29), 24799.
- Xu, Z.W., et al., 2022. *J. Mol. Struct.* 1254.
- Xu, H.T., et al., 2023. *Carbohydr. Polym.* 301.
- Yang, W.J., Zhao, X.B., 2019. *Mol. Pharmaceut.* 16 (6), 2826.
- Zhalechin, M., et al., 2021. *Heliyon* 7, 5.
- Zhang, Q.Q., et al., 2021. *Nanomaterials-Basel* 11, 9.